Nonlinear Dyn (2010) 60: 277–293
DOI 10.1007/s11071-009-9595-8

ORIGINAL PAPER

Nonlinear dynamics of an inclined beam subjected to a moving load

Ahmad Mamandi · Mohammad H. Kargarnovin · Davood Younesian

Received: 17 May 2009 / Accepted: 8 September 2009 / Published online: 6 October 2009

Abstract In this paper, the nonlinear dynamic response of an inclined pinned-pinned beam with a constant cross section, finite length subjected to a concentrated vertical force traveling with a constant velocity is investigated. The study is focused on the mode summation method and also on frequency analysis of the governing PDEs equations of motion. Furthermore, the steady-state response is studied by applying the multiple scales method. The nonlinear response of the beam is obtained by solving two coupled nonlinear PDEs governing equations of planar motion for both longitudinal and transverse oscillations of the beam. The dynamic magnification factor and normalized time histories of mid-pint of the beam are obtained for various load velocity ratios and the outcome results have been illustrated and compared to the results with those obtained from traditional linear solution. The appropriate parametric study considering the effects of the linear viscous damping, the velocity of the traveling load, beam inclination angle under zero or nonzero axial load are carried out to capture the influence of the effect of large deflections caused by stretching effects due to the beam's immovable ends. It was seen that quadratic nonlinearity renders the softening effect on the dynamic response of the beam under the act of traveling load. Also in the case where the object leaves the inclined beam, its planar motion path is derived and the targeting accuracy is investigated and compared with those from the rigid solution assumption. Moreover, the stability analysis of steady-state response for the modes equations having quadratic nonlinearity was carried out and it was observed from the frequency response curves that for the considered parameters in the case of internal-external primary resonance, both saturation phenomenon and jump phenomenon can be predicted for the longitudinal excitation.

Keywords Nonlinear vibrations · Inclined beam · Mode summation method · Frequency response analysis · Multiple scales method · Quadratic nonlinearity

A. Mamandi is a Ph.D. Student.

A. Mamandi · M.H. Kargarnovin (✉)
Mechanical and Aerospace Engineering Department, Science and Research Branch, Islamic Azad University, Tehran, Iran
e-mail: mhkargar@sharif.edu

A. Mamandi
e-mail: am_2001h@yahoo.com

M.H. Kargarnovin
Mechanical Engineering Department, Sharif University of Technology, Tehran, Iran

D. Younesian
Railway Engineering Department, Iran University of Science and Technology, Tehran, Iran

1 Introduction

The linear and nonlinear analysis for forced vibrations of structural elements, such as beams and plates under the act of traveling loads is of considerable practical importance. Many analytical and numerical methods have been proposed in the past decades to investigate the dynamic behavior of all customary and noncustomary shapes of isotropic material, and composite and FGM made engineering structural elements in the academic literatures. However, until now little attention has been paid to the study for dynamic response of the coupled longitudinal-transverse vibrations of an inclined beam subjected to a vertical concentrated moving load. Bridges on which vehicles or trains travel, and trolleys of overhead traveling cranes that move on their girders may be modeled as moving loads on simply supported beams. Also in aerospace industries, the rocket launcher systems and fire arms are some applications in vibration of inclined beams.

A comprehensive treatment of the subject of vibrations of structures due to moving loads which contains a large number of related cases is studied in [5]. In that those works are linear, nothing exists on the longitudinal motions of such a system. A common method to tackle issues of a moving force traveling on infinite length beams is the integral transforms [8]. On the other hand, in order to deal with problems including finite length beams, the modal analysis is commonly used. The linear dynamic analysis of a multispan beam traveled by a moving force with accelerating/decelerating velocity was studied in [14]. In [4], a dynamic Green function approach is used to determine the response of a simply supported Euler–Bernoulli beam of finite length subject to a moving load and authors proposed a simple matrix expression for the deflection of the beam. The effect of a moving mass on the dynamic behavior of a simply supported Euler–Bernoulli beam was studied in [15]. The linear finite element analysis was applied to analyze a simply supported Euler–Bernoulli beam under the act of moving loads by [7, 10, 12]. The dynamic behavior of a flexible cantilever beam carrying a moving mass-spring is investigated in [19]. In this paper, the dynamics of the system are described by coupled nonlinear partial differential equations and the equations of motion are solved numerically using the Galerkin method and an automatic ODE solver. The numerical results are compared with a closed-form analytical solution obtained using a perturbation method and the spectral behavior of the system are investigated using time-frequency analysis. The linear analysis was applied on a Timoshenko beam traversed a moving mass in [11] using the Galerkin's technique and the results of this work is verified by [13] using the linear finite element method. The effect of weight of the beam on the dynamic responses of a horizontal simply supported Timoshenko beam under the influence of moving forces was studied in [23] using the Galerkin's method. The linear moving mass problem for dynamic analysis of a Timoshenko beam is studied by [3]. In another work, the finite difference technique is used by [2] in dynamic analysis of a simple beam traversed by uniform partially moving masses. The dynamic behavior of the multispan continuous Euler–Bernoulli beam traversed by a moving mass at a constant velocity is investigated by [6] and the solution is obtained by using both eigenfunction expansion or the modal analysis method and the direct integration method in combination. Vibration of multispan Timoshenko beams and frames due to moving loads were studied by [22, 24], respectively. A simple procedure based on the finite element method has been developed for treating the dynamic analysis of beams on an elastic foundation subjected to moving point loads, where the foundation has been modeled by springs of variable stiffness in [21]. The closed-form solutions for the response of beams with general boundary conditions subjected to a single deterministic moving force are obtained by [1]. Analytic expressions of the dynamic amplification factor and the characteristic response spectrum are derived for weakly damped Euler–Bernoulli beams with various boundary conditions by [18]. The longitudinal and transverse motions of a finite length elastic Euler–Bernoulli beam traversed by a moving mass are studied in [26] using Hamilton's principle to obtain two nonlinear coupled differential equations governing the transverse and longitudinal displacements of the beam and a finite difference method combined with a perturbation technique is used to solve the resulting boundary value problem. In [17], the dynamic responses of a simply supported beam subjected to a constant velocity moving force is discussed and analytical and linear finite element solutions are presented. In [9, 28], nonlinear dynamical behavior of Timoshenko beams with infinite length under the act of traveling harmonic loads

resting on viscoelastic foundations are studied. Dynamic response of an inclined Euler–Bernoulli beam subjected to a moving mass has been investigated in [25] using the linear finite element method considering transversal and longitudinal displacements for the beam. In [27], the nonlinear vibration of a horizontal pinned-pinned thin beam under the act of a moving mass considering the influence of the load inertia and the nonlinearity caused by stretching effect of mid-plane of the beam due to the immovable supports was studied. Moreover, the effect of longitudinal inertia and longitudinal damping in governing equations of motion has been neglected and so their approximate-analytical solution is based on multiple times scale method for the system having nonlinearity. Recently, the nonlinear dynamic analysis of an eccentrically prestressed beam under the act of a concentrated moving harmonic load including damping effect has been studied in [20]. In that paper, the nonlinear deflections behavior of the beam is approximated by some polynomial functions and material of the beam was assumed to follow the Kelvin–Voigt model. Furthermore, the effects of large deflections, the internal damping of the beam, the velocity of the moving harmonic load, the prestress load, and the excitation frequency were discussed.

The main objective of this study is to focus on the influence of a moving load on the coupled PDEs governing equations of motion for an inclined beam considering longitudinal and transversal interaction of oscillations; in addition, to investigate on the behavior of frequency response for the system having quadratic non-linearity in its mode equations. Moreover, the stability analysis of steady-state response in the case of internal-external primary resonance and the influence of detuning parameter in the shape of modal response of the inclined beam under the act of traveling load are performed.

2 Modeling and mathematical formulation

A one-dimensional inclined beam of length l and inclination angle of θ traveled by a concentrated vertical force of F, which is always applied in Y direction, is considered (see Fig. 1a). The longitudinal and lateral components of traveling load in direction of x and y are $F\sin\theta$ and $F\cos\theta$, respectively (see Fig. 1b). In our up-coming analysis, it is assumed that when the force enters the left end of the beam, zero initial conditions are assumed, i.e., the beam is at rest at time $t = 0$. It is further assumed that the force will be in full contact with the beam during its motion, i.e., no separation occurs. The nonlinear dynamic behavior for the coupled longitudinal and transverse vibrations of an inclined uniform beam under simultaneous act of an axial force and transverse moving force is considered. The beam supports are restricted from any axial movement, and hence this will produce mid-plane stretching and some nonlinearity in governing equations of motion. For an Euler–Bernoulli beam, the governing coupled nonlinear partial differential equations of forced planar vibrations considering linear viscous damping are [16]

$$u_{tt} + \frac{c_1}{\rho A}u_t - \frac{E}{\rho}u_{xx} = \frac{(EA-P)}{\rho A}[w_x w_{xx}] - \frac{F\sin\theta}{\rho A}\delta(x-\varsigma) \tag{1}$$

and

$$w_{tt} + \frac{c_2}{\rho A}w_t - \frac{P}{\rho A}w_{xx} + \frac{EI}{\rho A}w_{xxxx} = \frac{(EA-P)}{\rho A}[u_{xx}w_x + u_x w_{xx}] - \frac{F\cos\theta}{\rho A}\delta(x-\varsigma) \tag{2}$$

in which $u = u(x,t)$ is the longitudinal time dependent deformation, $w = w(x,t)$ is the lateral time de-

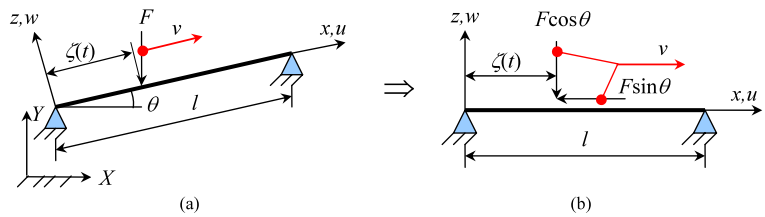

Fig. 1 (**a**) An inclined pinned-pinned beam subjected to a moving lateral load. (**b**) Equivalent moving load model

pendent deflection measured upward from its equilibrium position when unloaded, and the subscripts t and x stand for the derivative with respect to the time (t) and space coordinate (x) to the related order, respectively. In addition, ρ is the beam density, A, I are the area and moment of inertia of the beam cross section, E is Young's modulus, EI is the flexural rigidity of the beam, c_1 and c_2 are constant coefficients related to the structural damping of the beam namely μ, P is the prescribed axial load, F is the magnitude of the constant vertical lateral traveling force, and θ is the angle of inclination. Furthermore, $\delta(x-\zeta)$ is the Dirac's delta function in which ζ is the instantaneous position of the lateral force moving with the velocity of v on the beam such that $\zeta = vt$.

3 Solution method

One of the general routines in the traditional dynamic analysis of a continuum is the modal analysis in which the time-spatial response function will be expanded in terms of linear undamped natural modes of system obtained by neglecting the effects of foundation and damping terms. Moreover, it is well documented that the infinitesimal motions are well described by these eigenfunctions. In what follows, in order to clarify the problem under investigation, the conventional series expansion solution based on modal analysis approach also called the mode summation method is considered to analyze the vibration of a beam with pinned-pinned ends conditions under moving lateral and axial loads. According to the separation of variables approach, the response of our continuous system in terms of the linear free-oscillation modes can be assumed as follows [16]:

$$u(x,t) = \sum_{n=1}^{\infty} \xi_n(t) \sin\frac{n\pi x}{l} \tag{3}$$

$$w(x,t) = \sum_{n=1}^{\infty} \eta_n(t) \sin\frac{n\pi x}{l} \tag{4}$$

The boundary conditions for a pinned-pinned beam with immovable ends are expressed as

$$\begin{aligned} u(0,t) = u(l,t) = w(0,t) = w(l,t) = w_{xx}(0,t) \\ = w_{xx}(l,t) = 0 \end{aligned} \tag{5}$$

and initial conditions are

$$\begin{aligned} &w(x,0) = 0, \qquad w_t(x,0) = 0, \qquad u(x,0) = 0 \\ &u_t(x,0) = 0 \end{aligned} \tag{6}$$

Substituting (3) and (4) into (1) and (2) lead to:

$$\begin{aligned} &\sum_{m=1}^{\infty} \left(\ddot{\xi}_m + 2\mu\lambda_m\dot{\xi}_m + \lambda_m^2\xi_m\right) \sin\frac{m\pi x}{L} \\ &\quad = -\pi^3\kappa \sum_{m=1}^{\infty}\sum_{k=1}^{\infty} k^2 m \eta_m\eta_k \cdot \cos\frac{m\pi x}{l} \sin\frac{k\pi x}{l} \\ &\qquad - \frac{F\sin\theta}{\rho A}\delta(x-\varsigma) \end{aligned} \tag{7}$$

$$\begin{aligned} &\sum_{m=1}^{\infty} \left(\ddot{\eta}_m + 2\mu\omega_m\dot{\eta}_m + \omega_m^2\eta_m\right) \sin\frac{m\pi x}{l} \\ &\quad = -\pi^3\kappa \sum_{m=1}^{\infty}\sum_{k=1}^{\infty} mk \eta_k\xi_m \cdot \left(k\cos\frac{m\pi x}{l}\sin\frac{k\pi x}{l}\right. \\ &\qquad \left. + m\sin\frac{m\pi x}{l}\cos\frac{k\pi x}{l}\right) - \frac{F\cos\theta}{\rho A}\delta(x-\varsigma) \end{aligned} \tag{8}$$

in which

$$\begin{aligned} &\omega_m = \frac{m\pi}{l}\left(\frac{EI}{\rho A}\frac{m^2\pi^2}{l^2} + \frac{P}{\rho A}\right)^{1/2} \\ &\lambda_m = \frac{m\pi}{l(\rho A)^{1/2}} \quad \text{and} \quad \kappa = \frac{EA-P}{\rho A l^3} \end{aligned} \tag{9}$$

Multiplying both sides of (7) and (8) by $\sin(n\pi x/l)$ and integrating over the interval $[0, l]$ lead:

$$\begin{aligned} &\ddot{\xi}_n + 2\mu\lambda_n\dot{\xi}_n + \lambda_n^2\xi_n \\ &\quad = \frac{-2F\sin\theta}{\rho A l}\sin\frac{n\pi vt}{l} - \frac{n\pi^3}{4} \\ &\qquad \times \kappa \sum_{m=1}^{\infty} m\eta_m\left[|n-m|\eta_{|n-m|} + (m+n)\eta_{m+n}\right] \end{aligned} \tag{10}$$

$$\begin{aligned} &\ddot{\eta}_n + 2\mu\omega_n\dot{\eta}_n + \omega_n^2\eta_n \\ &\quad = \frac{-2F\cos\theta}{\rho A l}\sin\frac{n\pi vt}{l} - \frac{n\pi^3}{4} \\ &\qquad \times \kappa \sum_{m=1}^{\infty} m\xi_m\left[|n-m|\eta_{|n-m|} + (m+n)\eta_{m+n}\right] \end{aligned} \tag{11}$$

4 Numerical results

Equations (10) and (11) are solved numerically using the fourth order Runge–Kutta method via MATLAB solver package out of which the values of $\xi_n(t)$ and $\eta_n(t)$ are obtained and then having on hand these values $u(x,t)$ and $w(x,t)$ can be calculated using (3) and (4). The numerical outcome of these procedures is presented in Figs. 2, 3, 4, 5, 6.

In the next step, the dynamic response of the beam under variation of different parameters namely; velocity of the concentrated moving force, axial load, modal damping, beam's inclination angle, and magnitude of the moving force are studied. To verify the accuracy of the obtained results some special cases are considered. For the linear case, we set higher order terms in (1) and (2) equal to zero which yield exactly to the linear solutions reported by Fryba [5] (see Fig. 2). However, as described in the Introduction section, to date no work on the nonlinear analysis of coupled longitudinal-transversal vibrations of inclined beams under the act of traveling load is reported.

In all following studied cases, the beam specifications are as follows unless otherwise specified: a beam with square cross-section having area of $A = 196 \times 10^{-4}$ m^2, $E = 200 \times 10^9$ N/m^2, $\rho = 7850$ kg/m^3 (steel), $l = 8$ m, $\mu = 0.033$ [27].

Let us define the dynamic magnification factor D_d as the ratio of the maximum magnitude of the dynamic deflection at the mid-span of the beam to the maximum static deflection at the same location. Also let us define the velocity ratio as $\alpha = \frac{v}{v_f} = \frac{T_f}{T}$ where T_f, T and v_f denote the first natural period (fundamental period of the transverse motion) of the beam, the total time taken by the moving load to cross from one end to the other beam's end and the velocity of a reference load that would take the time of T_f to traverse the beam of length l, respectively.

Figure 2 shows the variation of the D_d vs. α for different values of the moving load for a horizontal beam. It can be seen that by increasing the magnitude of the vertical moving load the dynamic displacement response of the beam grows in such a way that does not follow the well-known linear force-deflection relation in the liner systems, i.e., $F = k\delta$. It can be observed that the dynamic displacement response of the linear and nonlinear solutions are almost the same for $F \leq 6000$ N and the maximum D_d for linear and nonlinear solutions are the same and equals to 1.73 at $\alpha = 1.2$ as reported by other researchers [17]. However, from this figure, it is clear that for the value of $F > 6000$ N the dynamic response of the beam using nonlinear theory has higher value than those given

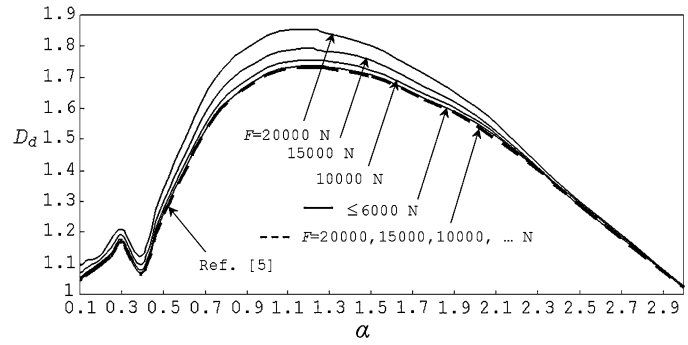

Fig. 2 Dynamic magnification factor (D_d) for mid-point of a horizontal steel beam vs. α for $l = 8$ m, $P = 0$, $\mu = 0$; (- - - - -) linear solution [5], (——) nonlinear analysis

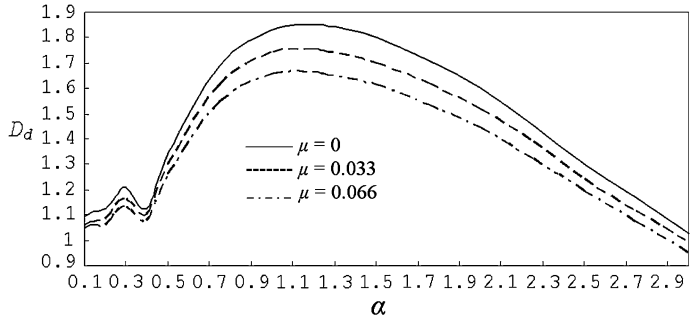

Fig. 3 Dynamic magnification factor (D_d) for mid-point of a horizontal steel beam vs. α for various damping coefficients using nonlinear analysis for $l = 8$ m, $F = 20000$ N, $P = 0$; (——) $\mu = 0$, (- - - - -) $\mu = 0.033$, (— · —) $\mu = 0.066$

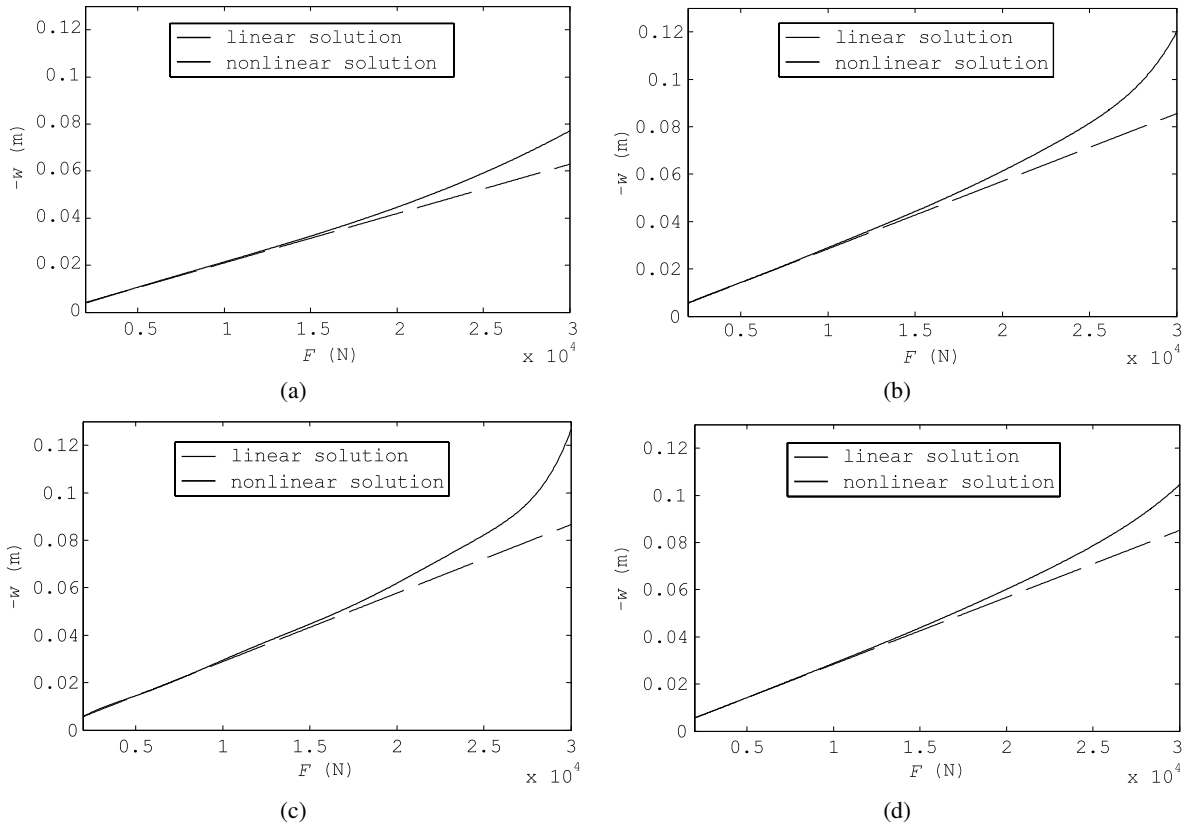

Fig. 4 Variation of the beam's mid-point dynamic displacement vs. magnitude of the moving load for different load velocities. $l = 8$ m, $A = 0.0196$ m^2, $\mu = 0$, $\theta = 0°$, $v_f = 40.04$ m/s; (**a**) $\alpha = 0.5$, (**b**) $\alpha = 1$, (**c**) $\alpha = 1.2$, (**d**) $\alpha = 1.5$; (- - - - -) linear, (——) nonlinear

by linear theory, hence the difference between the dynamic displacement responses of the nonlinear and linear theories increase. The reason for this deviation is due to effect of larger deflection on the higher values of the transverse traveling force. Furthermore, as seen from Fig. 2, the velocity of the moving load plays an important role on the dynamic displacement response. For example, the maximum value of the dynamic magnification factor D_d is about 1.85 when $F = 20000$ N at $\alpha = 1.2$. Meanwhile, in the region $0 < \alpha < 1.2$, one can observe another maximum around $\alpha = 0.3$ a phenomenon which is also reported by other researchers [17]. Briefly it can be said that in the under critical region ($\alpha \leq 1.2$) the dynamic deflection of the beam generally increases by increasing the velocity of the load and in the overcritical region ($\alpha > 1.2$), the dynamic deflection decreases by increasing the velocity of the traveling load.

Figure 3 shows the effect of modal damping on the dynamic behavior of mid-point of a horizontal steel beam under study using nonlinear analysis. Three different values of μ including $\mu = 0$ (undamped condition), 0.033, and 0.066 have been considered. From this figure, it can be said that by increasing the value of damping coefficient μ, the dynamic displacement decreases which is generally a natural phenomenon in any structural system. Furthermore, for the considered parameters, the maximum value of D_d decreases from 1.85 (related to $\mu = 0$) to 1.66 (related to $\mu = 0.066$) at $\alpha = 1.2$.

In Fig. 4, the beam's mid-point dynamic displacement using both linear and nonlinear approaches under different values of the moving load have been extracted for various velocity ratios of $\alpha = 0.5$, 1, 1.2, 1.5, respectively. It can be seen that the dynamic deflection of the nonlinear analysis is higher than the one obtained from the linear solution. This incident is known as the softening behavior which is mostly due to the existence of the quadratic nonlinearity characteristic in the beam's mode equations of motion, and

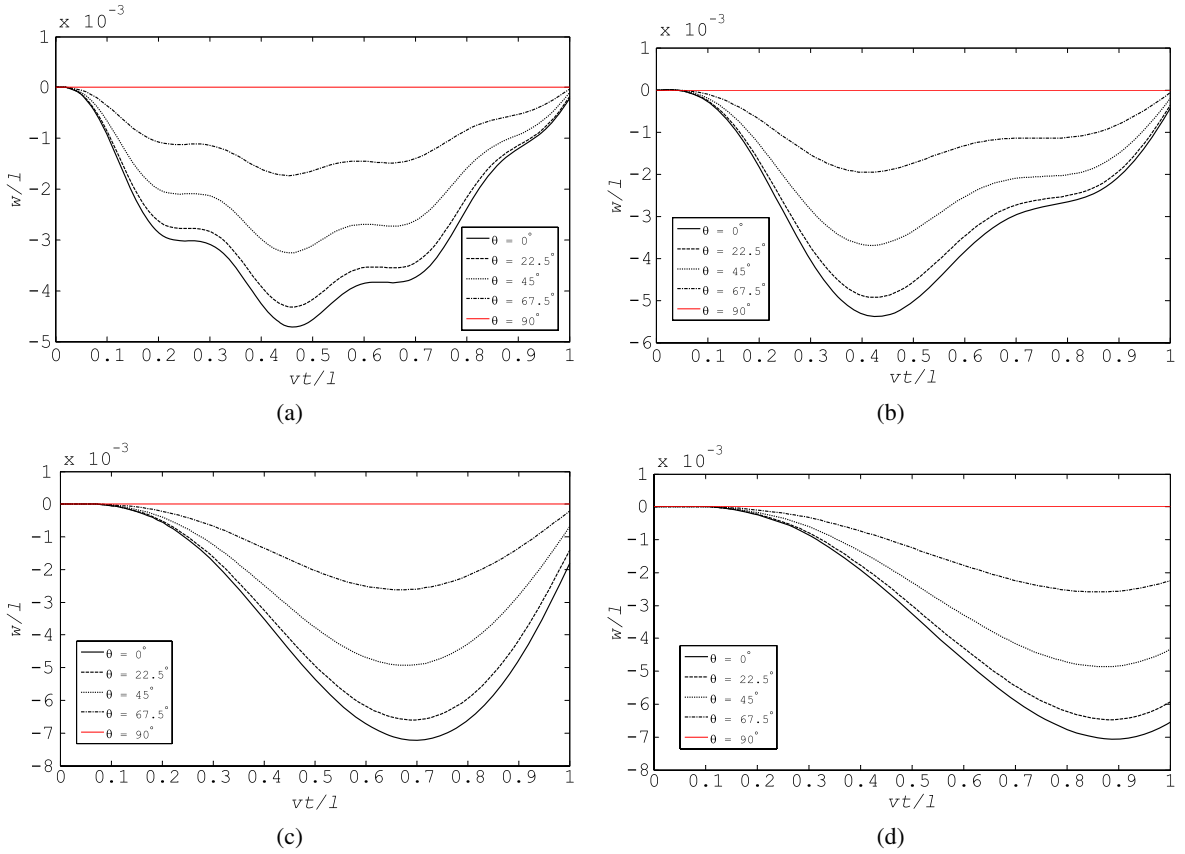

Fig. 5 Time histories for normalized mid-span deflection for: $l = 8$ m, $F = 20000$ N, $P = 3000$ N, $\mu = 0.033$, $v_f = 40.04$ m/s; (**a**) $\alpha = 0.25$, (**b**) $\alpha = 0.5$, (**c**) $\alpha = 1$, (**d**) $\alpha = 1.5$

hence this system is taken to be equivalent to a nonlinear soft spring [16]. Also, it is seen from this figure that the dynamic mid-point displacement of such beam using linear and nonlinear solutions are almost the same for the value of $F \leq 10000$ N. However, after this value of F, the magnitude of the w of the linear and the nonlinear solutions differs gradually and the difference becomes more as F increases. Also, it can be observed from Fig. 4 that the difference between the linear and the nonlinear solutions has an increasing trend up to the load velocity ratio of $\alpha = 1.2$ and illustrates a reverse trend for the load velocity ratio of $\alpha > 1.2$. Note that the maximum difference of all cases in this figure between linear and nonlinear solutions occurs at $F = 30000$ N and at $\alpha = 1.2$ (see Fig. 4c).

Figures 5a–d show time histories for normalized dynamic deflection of mid-point of the beam for different values of beam's inclination angle ($\theta = 0°$, 22.5°, 45°, 67.5°, and 90°) vs. nondimensional time vt/l, where t denotes the time duration of the moving load from the time it enters over the beam and for different velocity ratios ($\alpha = 0.25$, 0.5, 1, 1.5). A close inspection of each figure in Figs. 5a–d reveals that by increasing the beam's inclination angle the dynamic displacement of mid-point of the beam decreases and, for example, at $\theta = 90°$, the dynamic lateral displacement becomes zero as expected. Furthermore, it can be seen from each figure that the peak point of each curve occurs at the same vt/l, no matter what the beam inclination angle would be.

Here, in order to give a an initial feeling to the readers about the CPU time for solution of the coupled differential equations, we ran the MATLAB code on a computer with the following specification: Intel (R) core 2 Duo CPU, E4500 @ 2.20 GHz and 1.00 GB RAM and the following corresponding CPU times were obtained for some cases regarding to this figure:

case 1: for $\alpha = 0.25, \theta = 0°$; we got: CPU time = 6.9688 s.

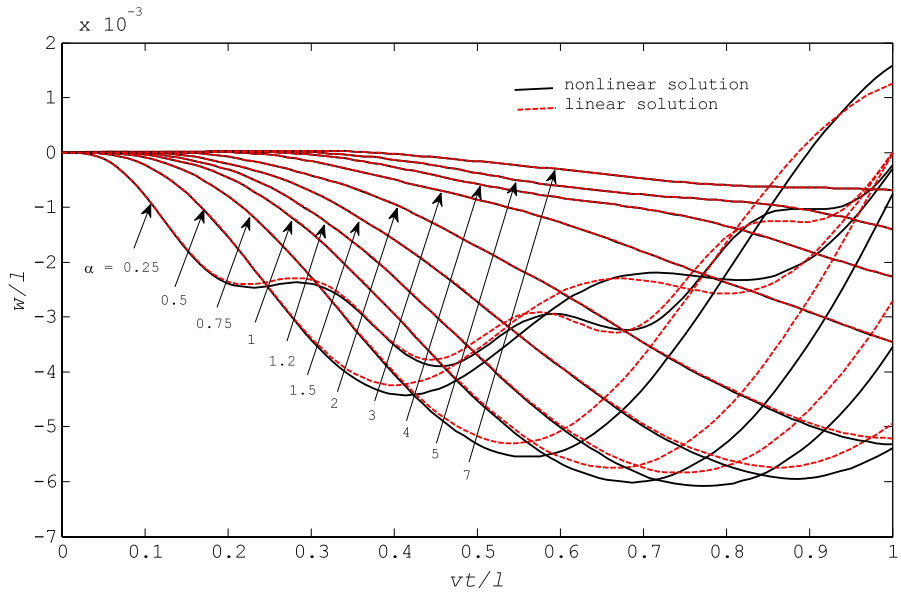

Fig. 6 Time history for deflection of the beam's mid-point vs. vt/l for different values of α, $l = 8$ m, $F = 20000$ N, $P = 0$, $\mu = 0$, $\theta = 36°$

case 2: for $\alpha = 1.5, \theta = 0°$; we got: CPU time = 1.7031 s.

It should be further noted that the interval of $[0, l/v]$ was divided into 1000 (number of time steps) intervals.

Figure 6 illustrates the variation of w/l of mid-point of the beam vs. vt/l for beam's inclination angle of $\theta = 36°$ for different load traveling velocity ratios. From the same figure, one can conclude that the results from the nonlinear dynamic analysis represent larger values for the lateral dynamic displacement of the beam compared to those calculated by linear analysis. Also, it can be seen that the peak value of each curve does not occur at the same vt/l, changing the values of these peak points have an increasing trend up to the load velocity ratio of $\alpha = 1.2$ and a reverse trend afterward. For the load velocity ratio of $\alpha \geq 0.75$, the position of the peak point shifts to the right as α increases. In addition, it is seen that for higher velocity ratio, i.e., $\alpha \geq 3$, the lateral dynamic displacement of the beam's mid-point yields to a very small value which means that the beam does not have enough time to respond accordingly against the load action. Another interesting observation from Fig. 6 is related to the interaction between beam's mid-point displacement and load speed when one deals for example with the load velocity of $\alpha = 0.75$ in which, there is a reverse (upward) displacement for the mid-point which happens usually when the load leaves the beam. Finally, the maximum downward beam's mid-point dynamic displacement occurs while the force leaves the beam with velocity ratio of $\alpha = 1.5$.

Case study: accuracy of targeting of a projectile leaving the tip of an inclined beam

The general application of this study can be addressed to the military and aerospace industries; more specifically, to the dynamic analysis of any kind of low size to high size caliber ammunition used in different types of fire arms weaponry. Consider a planar motion of a simple projectile having a known velocity when it leaves the tip of an inclined beam (see Fig. 7). In practice, the analysis of projectile motion is done using the rigid beam model, whereas in reality the beam is a flexible structure. Usually at a situation like this, the accuracy of expected collision point is the most principal objective for this kind of motion. Since we are not going to consider the beam as a rigid continuum, therefore, one deals with a specific beam slope at the end support when the projectile leaves the beam. Indeed, the size of this slope will play a significant role in the target accuracy. We intend to show the effect of this slope on the target accuracy using nonlinear analysis. Suppose that point p_1 is the position of collision predicted by the rigid (classical) type of analysis and point p_2 the same point predicted by the nonlinear analysis under beam's inclination angle of θ_{rigid} and beam's end slope of θ_{endslope}, respectively (see Fig. 7).

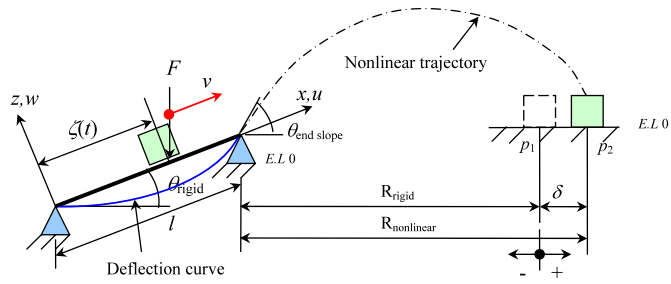

Fig. 7 Prediction of a planar motion of a projectile using different theories

Table 1 δ distance in targeting of planar projectile on an inclined steel beam for various moving load velocity ratios ($I = 171 \times 10^{-8}$ m^4, $A = 10.3 \times 10^{-4}$ m^2, $l = 5$ m, $\mu = 0$, $F = 3000$ N, $P = 0$, $v_f = 64.54$ m/s)

Velocity ratio	δ (+ or −) (m) due to $F = 3000$ N		
α	$\theta = 36°$	$\theta = 45°$	$\theta = 54°$
4.25	48.95	−1.33	−37.60
4.5	52.14	−1.35	−39.95
4.75	56.09	−1.39	−42.89
5	60.59	−1.47	−46.28
5.25	63.22	−1.44	−48.17
5.5	64.01	−1.34	−48.59

As a classical case study, Table 1 shows the calculated results for the difference in target position δ ($\delta = R_{\text{nonlinear}} - R_{\text{rigid}}$) vs. the velocity ratios α for a beam with different inclination angles of $\theta_{\text{rigid}} = 36°$, 45°, and 54°, respectively. The following data is used for this case study: $I = 171 \times 10^{-8}$ m^4, $A = 10.3 \times 10^{-4}$ m^2, $l = 5$ m, $\mu = 0$, $F = 3000$ N, $P = 0$.

To illustrate the effect of considering the slope of the beam at the time when the projectile leaves the tip of the beam, consider an instance where $\alpha = 5.5$ and $\theta_{\text{rigid}} = 36°$, and keeping all other parameters the same, the difference in target position with respect to the rigid beam assumption is: $R_{\text{nonlinear}} - R_{\text{rigid}} = 64.01$ m about 0.53% error (see Fig. 7). As it is seen from Table 1 under considered range for the velocity ratios, the maximum absolute values of δ occur at $\alpha = 5.5$ at $\theta = 36°$. Moreover, this table further reveals that the comparison of the δ values for three different inclination angles, has its absolute least values for $\theta = 45°$at any velocity ratios.

5 Frequency and stability analysis of forced oscillations of an inclined beam

In this section primarily we try to obtain the differential equations for the time varying part of motion equations of an inclined beam with linear viscous damping under the act of traveling load using multiple scales method. Then the internal-external primary resonance analysis of the forced response considering coupled longitudinal and transverse oscillations will be carried out.

To make this analysis more convenient, following dimensionless variables are defined [16]:

$$X = \frac{x}{l}, \qquad \tau = \frac{r_g}{l^2}\sqrt{\frac{E}{\rho}}t, \qquad N = \frac{Pl^2}{r_g^2 EA}$$
$$W = \frac{w}{l}, \qquad U = \frac{u}{l}, \qquad r = \frac{r_g}{l}$$

where r_g is the radius of gyration of the beam. Consequently, the dimensionless forms of (10) and (11) can be written as

$$\ddot{\xi}_n + \frac{2\nu_n}{r^2}\dot{\xi}_n + \lambda_n^2\xi_n = \frac{g\sin(n\pi V\tau)}{r^2} - \frac{n\pi^3\kappa}{4r^2}\sum_{m=1}^{\infty} m\eta_m\big[|n-m|\eta_{|n-m|} + (m+n)\eta_{m+n}\big] \tag{12}$$

$$\ddot{\eta}_n + 2\mu_n\dot{\eta}_n + \omega_n^2\eta_n = \frac{f\sin(n\pi V\tau)}{r^2} - \frac{n\pi^3\kappa}{4r^2}\sum_{m=1}^{\infty} m\xi_m\big[|n-m|\eta_{|n-m|} + (m+n)\eta_{m+n}\big] \tag{13}$$

where $f=\frac{-2F\cos\theta}{EA}$, $g=\frac{-2F\sin\theta}{EA}$, $\kappa=1-r^2N$, $\omega_n=n\pi\times(n^2\pi^2+N)^{\frac{1}{2}}$ and $\lambda_n=n\pi/r$. Let us define parameter ε then we introduce the following new parameters as

$$\begin{aligned}&\hat{\xi}_n=\frac{\xi_n}{\varepsilon},\qquad \hat{\eta}_n=\frac{\eta_n}{\varepsilon},\qquad \varepsilon\hat{v}_n=r^{-2}v_n\\&\varepsilon\hat{\mu}_n=\mu_n,\qquad \varepsilon\hat{g}_n=r^{-2}g_n\\&\varepsilon\hat{f}_n=r^{-2}f_n,\quad \text{and}\quad \hat{\kappa}=\pi^3\kappa\left(4r^2\right)^{-1}\end{aligned}\tag{14}$$

in which $f_n=f\sin(n\pi V\tau)$ and $g_n=g\sin(n\pi V\tau)$. After substituting ξ_n, η_n, v_n, μ_n, and κ from above relation into (12) and (13) and for the simplicity dropping the hats sign in the results, one would get the quadratic nonlinear mode equations as [16]

$$\begin{aligned}\ddot{\xi}_n+\lambda_n^2\xi_n=\varepsilon\Bigg[&-2v_n\dot{\xi}_n-n\kappa\sum_{m=1}^{\infty}m\eta_m(p\eta_p+q\eta_q)\Bigg]\\&-\varepsilon g\cos(n\pi V\tau+\pi/2)\end{aligned}\tag{15}$$

$$\begin{aligned}\ddot{\eta}_n+\omega_n^2\eta_n=\varepsilon\Bigg[&-2\mu_n\dot{\eta}_n-n\kappa\sum_{m=1}^{\infty}m\xi_m(p\eta_p+q\eta_q)\Bigg]\\&-\varepsilon f\cos(n\pi V\tau+\pi/2)\end{aligned}\tag{16}$$

where $p=|n-m|$ and $q=n+m$. We use the method of multiple scales and seek an approximate solution of (15) and (16) for small but finite amplitudes in the form of

$$\begin{aligned}&\xi_n(\tau,\varepsilon)=\xi_{n0}(\tau_0,\tau_1)+\varepsilon\xi_{n1}(\tau_0,\tau_1)+O\left(\varepsilon^2\right)\\&\eta_n(\tau,\varepsilon)=\eta_{n0}(\tau_0,\tau_1)+\varepsilon\eta_{n1}(\tau_0,\tau_1)+O\left(\varepsilon^2\right)\end{aligned}\tag{17}$$

where $\tau_n=\varepsilon^n\tau$, i.e., $\tau_0=\tau$ and $\tau_1=\varepsilon\tau$, represents different independent time scales. Substituting (17) into (15) and (16) and noting that $d/d\tau=D_0+\varepsilon D_1+\cdots$, $d^2/d\tau^2=D_0^2+2\varepsilon D_0D_1+\cdots$, where $D_0=d/d\tau$, $D_1=d/d\tau_1$ and equating coefficients of like powers of ε, we obtain the following set of second-order ordinary differential equations:

$$O\left(\varepsilon^0\right):\begin{cases}D_0^2\xi_{n0}+\lambda_n^2\xi_{n0}=0\\D_0^2\eta_{n0}+\omega_n^2\eta_{n0}=0\end{cases}\tag{18}$$

$$O(\varepsilon):\begin{cases}D_0^2\xi_{n1}+\lambda_n^2\xi_{n1}\\\quad=-2D_0D_1\xi_{n0}-2v_nD_0\xi_{n0}\\\qquad-n\kappa\sum_{m=1}^{\infty}m\eta_{m0}(p\eta_{p0}+q\eta_{q0})\\\qquad-g\cos(\Omega_n\tau+\pi/2)\\D_0^2\eta_{n1}+\omega_n^2\eta_{n1}\\\quad=-2D_0D_1\eta_{n0}-2\mu_nD_0\eta_{n0}\\\qquad-n\kappa\sum_{m=1}^{\infty}m\xi_{m0}(p\eta_{p0}+q\eta_{q0})\\\qquad-f\cos(\Omega_n\tau+\pi/2)\end{cases}\tag{19}$$

where $\Omega_n=n\pi V$ $(n=1,2,3,\ldots)$. The solution of (18) can be written in the form [16]:

$$\begin{aligned}&\xi_{n0}=A_n(\tau_1)\exp(i\lambda_n\tau_0)+c.c.\\&\eta_{n0}=B_n(\tau_1)\exp(i\omega_n\tau_0)+c.c.\end{aligned}\tag{20}$$

Now by substituting ξ_{n0}, η_{n0} from (20) into (19) one would get

$$O(\varepsilon):\begin{cases}D_0^2\xi_{n1}+\lambda_n^2\xi_{n1}\\\quad=-2i\lambda_n(D_1A_n+v_nA_n)\exp(i\lambda_n\tau_0)\\\qquad-n\kappa\sum_{m=1}^{\infty}mB_m\big\{pB_p\exp\big[i(\omega_m+\omega_p)\tau_0\big]\\\qquad+p\bar{B}_p\exp\big[i(\omega_m-\omega_p)\tau_0\big]\\\qquad+qB_q\exp\big[i(\omega_m+\omega_q)\tau_0\big]\\\qquad+q\bar{B}_q\exp\big[i(\omega_m-\omega_q)\tau_0\big]\big\}\\\qquad-\frac{g}{2}\exp\big[i(\Omega_n\tau+\pi/2)\big]+c.c.\end{cases}\tag{21}$$

$$O(\varepsilon):\begin{cases}D_0^2\eta_{n1}+\omega_n^2\eta_{n1}\\\quad=-2i\omega_n(D_1B_n+\mu_nB_n)\exp(i\omega_n\tau_0)\\\qquad-n\kappa\sum_{m=1}^{\infty}mA_m\big\{pB_p\exp\big[i(\lambda_m+\omega_p)\tau_0\big]\\\qquad+p\bar{B}_p\exp\big[i(\lambda_m-\omega_p)\tau_0\big]\\\qquad+qB_q\exp\big[i(\lambda_m+\omega_q)\tau_0\big]\\\qquad+q\bar{B}_q\exp\big[i(\lambda_m-\omega_q)\tau_0\big]\big\}\\\qquad-\frac{f}{2}\exp\big[i(\Omega_n\tau+\pi/2)\big]+c.c.\end{cases}\tag{22}$$

The $c.c.$ symbol and equivalently bar sign over any parameters indicate that parameter is a complex con-

jugate term. It can be proven that when $\lambda_n \simeq \omega_m \pm \omega_p$ or $\lambda_n \simeq \omega_m \pm \omega_q$ in (21) and (22), an extra link exists which connects ξ_{n1} and η_{n1}. Under this condition, an internal resonance will be formed.

To analyze the particular solutions of (21) and (22), we need to distinguish between the internal resonant case and the nonresonant case. These special cases are described in the next sections.

5.1 The nonresonant condition

In this case, the only terms that produce secular terms are the terms proportional to $\exp(i\lambda_n\tau_0)$ in (21) and the terms proportional to $\exp(i\omega_n\tau_0)$ in (22), thus the solvability conditions become

$$D_1 A_n + \nu_n A_n = 0 \quad \text{and} \quad D_1 B_n + \mu_n B_n = 0 \tag{23}$$

it follows that

$$\begin{aligned} A_n &= a_n \exp(-\nu_n \tau_1) \quad \text{and} \\ B_n &= b_n \exp(-\mu_n \tau_1) \end{aligned} \tag{24}$$

where a_n and b_n are complex constants and

$$\begin{aligned} \xi_n &= \exp(-\varepsilon\nu_n\tau)\big[a_n \exp(i\lambda_n\tau) + c.c.\big] + O(\varepsilon) \\ \eta_n &= \exp(-\varepsilon\mu_n\tau)\big[b_n \exp(i\omega_n\tau) + c.c.\big] + O(\varepsilon) \end{aligned} \tag{25}$$

the steady-state solutions can be obtained when $\tau \to \infty$, i.e.,

$$\xi_n = \eta_n = 0 \tag{26}$$

5.2 The resonant condition

In this section, we consider two different resonance conditions, namely:

(a) The longitudinal primary external resonance.
(b) The internal–external longitudinal primary resonance.

(a) *Longitudinal primary external resonance*

Let us consider a case where Ω_n is near the λ_n. Furthermore, we introduce an external detuning parameter σ_1 such that

$$\Omega_n = \lambda_n + \varepsilon\sigma_1 \tag{27}$$

By introducing above Ω_n into (21) and (22), it can be seen that none of the nonlinear terms produce a secular term, and the solvability conditions are

$$\begin{aligned} &-2i\lambda_n(D_1 A_n + \nu_n A_n) \\ &\quad -\frac{g}{2}\exp\big[\exp i(\sigma_1\tau_1 + \pi/2)\big] = 0 \quad \text{and} \\ &D_1 B_n + \mu_n B_n = 0 \end{aligned} \tag{28}$$

the solutions of above relations yield to

$$\begin{aligned} A_n &= \frac{1}{2}a_n \exp(-\nu_n\tau_1 + i\alpha_n) + \frac{ig}{4(\nu_n + i\sigma_1)\lambda_n} \\ &\quad \times \exp\big[i(\sigma_1\tau_1 + \pi/2)\big] \\ B_n &= \frac{1}{2}b_n \exp(-\mu_n\tau_1 + i\beta_n) \end{aligned} \tag{29}$$

where α_n and β_n are constants. As $\tau \to \infty$, then $\tau_1 \to \infty$, so we have

$$\begin{aligned} A_n &\to \frac{ig}{4(\nu_n + i\sigma_1)\lambda_n}\exp\big[i(\sigma_1\tau_1 + \pi/2)\big] \quad \text{and} \\ B_n &\to 0 \end{aligned} \tag{30}$$

Substituting (30) into (20) and (17) and expressing the result in terms of the original variables, one would get the following steady-state response:

$$\begin{aligned} \xi_n &= \xi_{n0} + O(\varepsilon) = -\frac{g}{2(\nu_n^2 + \sigma_1^2)^{1/2}\lambda_n} \\ &\quad \times \sin\left[\Omega_n\tau + \pi/2 - \arctan\left(\frac{\sigma_1}{\nu_n}\right)\right] + O(\varepsilon) \\ \eta_n &= \eta_{n0} + O(\varepsilon) = 0 \end{aligned} \tag{31}$$

A close inspection of above solution reveals that in the case of no internal resonance, i.e., $\lambda_n \neq \omega_m \pm \omega_p$ or $\lambda_n \neq \omega_m \pm \omega_q$, the first approximation will not be affected by the nonlinear terms, hence the resulting relation represents essentially the solution of a linear problem.

(b) *Internal–external primary resonance in longitudinal excitation*

Internal resonance could be described by [16]: $\lambda_n \cong \omega_m \pm \omega_p$ and or $\lambda_n \cong \omega_m \pm \omega_q$ and longitudinal primary *External* resonance condition would be defined when $\Omega_n \cong \lambda_n$. As a case study, we consider the condition for internal resonance as $\lambda_n \cong \omega_m + \omega_p$

and external resonance as defined before the solvability conditions of (21) and (22) are

$$\begin{aligned}
&-2i\lambda_n(D_1A_n+\nu_nA_n)-n\kappa\sum_{m=1}^{\infty}mpB_mB_p\\
&\quad\times\exp(-i\sigma_2\tau_1)-\frac{g}{2}\exp\big[i(\sigma_1\tau_1+\pi/2)\big]=0\\
&-2i\omega_n(D_1B_n+\mu_nB_n)\\
&\quad-nk\sum_{m=1}^{\infty}mpA_m\bar{B}_p\exp(i\sigma_2\tau_1)=0
\end{aligned}\tag{32}$$

where

$$\Omega_n=\lambda_n+\varepsilon\sigma_1\quad\text{and}\quad\lambda_n=\omega_m+\omega_p+\varepsilon\sigma_2\tag{33}$$

in which σ_2 is the internal detuning parameter. We introduce the polar notation for amplitudes as

$$A_n=\frac{1}{2}a_n\exp(i\alpha_n)\quad\text{and}\quad B_n=\frac{1}{2}b_n\exp(i\beta_n)\tag{34}$$

where a_n, b_n, α_n, and β_n are real function of τ_1. Now, to have a better intuition of what is happening, we input $n=1$, $m=2$ and $p=3$ in (32)–(34), after doing some manipulations, separating real and imaginary parts, and mathematical simplifications the following differential algebraic equations (DAEs) are obtained [16]:

$$\begin{aligned}
a_1'&=-\nu_1a_1+\frac{3\kappa}{2\lambda_1}b_2b_3\sin\gamma_2-\frac{g}{2\lambda_1}\sin\gamma_1\\
&=f_1(a_1,b_2,b_3,\gamma_1,\gamma_2)\\
b_2'&=-\mu_2b_2-\frac{3\kappa}{2\omega_2}a_1b_3\sin\gamma_2\\
&=f_2(a_1,b_2,b_3,\gamma_1,\gamma_2)\\
b_3'&=-\mu_3b_3-\frac{3\kappa}{2\omega_3}a_1b_2\sin\gamma_2\\
&=f_3(a_1,b_2,b_3,\gamma_1,\gamma_2)\\
\gamma_1'&=\sigma_1-\frac{3\kappa}{2\lambda_1a_1}b_2b_3\cos\gamma_2-\frac{g}{2\lambda_1a_1}\cos\gamma_1\\
&=f_4(a_1,b_2,b_3,\gamma_1,\gamma_2)\\
\gamma_2'&=\sigma_2+\frac{3\kappa}{2}\left(\frac{b_2b_3\cos\gamma_2}{\lambda_1a_1}-\frac{a_1b_3\cos\gamma_2}{\omega_2b_2}\right.\\
&\quad\left.-\frac{a_1b_2\cos\gamma_2}{\omega_3b_3}\right)+\frac{g}{2\lambda_1a_1}\cos\gamma_1\\
&=f_5(a_1,b_2,b_3,\gamma_1,\gamma_2)
\end{aligned}\tag{35}$$

in which

$$\begin{aligned}
&\gamma_1=\sigma_1\tau_1-\alpha_1+\pi/2\quad\text{and}\\
&\gamma_2=\sigma_2\tau_1+\alpha_1-\beta_2-\beta_3
\end{aligned}\tag{36}$$

where other cases could be treated the same. For the steady-state response, we set $a_1'=b_2'=b_3'=\gamma_1'=\gamma_2'=0$ in (35) and (36). Note that the prime over any parameter denotes the first derivative with respect to τ_1.

To check the stability condition of the steady-state solution, we linearize (35) and (36) near the singular (or steady-state) points. This will lead to a set of linear equations having constant coefficients multiplied by unknown disturbance terms. In other words, this is a typical case known as eigenvalue problem. If the real part of each eigenvalue of the coefficient matrix is not positive then the point is stable otherwise is unstable. Having on hand the values of a_1, b_2, b_3, γ_1, and γ_2, we assume that each of them is comprised of two parts; i.e., a steady-state part (fixed point or singular point) and a disturbance part. By employing this technique, we have $a_1=a_{10}+a_{11}$, $b_2=b_{20}+b_{21}$, $b_3=b_{30}+b_{31}$, $\gamma_1=\gamma_{10}+\gamma_{11}$ and $\gamma_2=\gamma_{20}+\gamma_{21}$, in which a_{10}, b_{20}, b_{30}, γ_{10}, and γ_{20} are the singular points in which their first derivative with respect to τ_1 are zero, and a_{11}, b_{21}, b_{31}, γ_{11} and γ_{21} are the disturbance parts of a_1, b_2, b_3, γ_1 and γ_2, respectively.

Now, to determine the nature of any various singular points we substitute the new forms a_1, b_2, b_3, γ_1 and γ_2 and their derivatives into (35) and (36), expanding the relations one can solve the linearized form of equations such as $\{\dot{\mathbf{X}}\}=[\mathbf{A}]\{\mathbf{X}\}$ to obtain the eigen-values where $\vec{\mathbf{X}}=\lfloor a_{11}\ b_{21}\ b_{31}\ \gamma_{11}\ \gamma_{21}\rfloor$ and $A_{ij}=\frac{\partial f_i(a_1,b_2,b_3,\gamma_1,\gamma_2)}{\partial x_j}|_{(a_{10},b_{20},b_{30},\gamma_{10},\gamma_{20})}$ with i, $j=1,2,\ldots,5$ (i.e. A_{ij} is the coefficient matrix defined about fixed points). Afterwards by solving: $\det([\mathbf{A}]-\lambda[\mathbf{I}])=0$, the eigenvalues ($\lambda_i$) to check the stability near singular points will be on hand, where $[\mathbf{I}]$ is identity matrix. Note that dot over the vector function of amplitude and phase denotes the first derivative with respect to τ_1.

In order to obtain the amplitude and frequency response curves, we need to solve (35) and (36). It follows that there are two possible solutions: either $a_1\neq0$ and $b_2=b_3=0$, or a_1, b_2 and b_3 are all nonzero. When $b_2=b_3=0$, the analytical solution of a_1 will be in the form: $a_1=\frac{g}{\lambda_1(\nu_1^2+\sigma_1^2)^{1/2}}$ which is

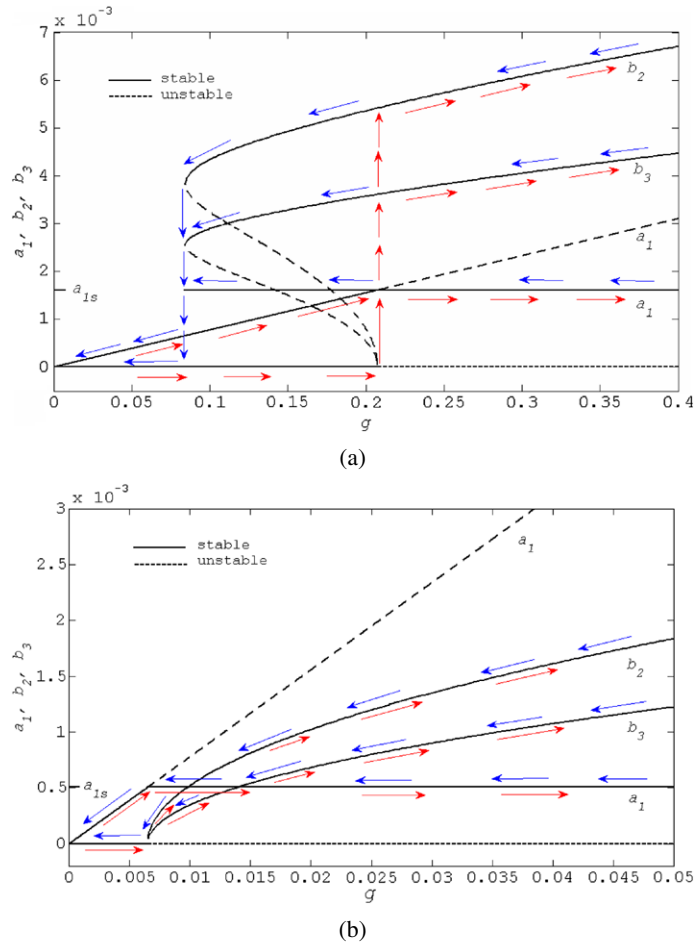

Fig. 8 Variation of a_1, b_2 and b_3 (Amplitude response) vs. g for an inclined pinned-pinned beam-longitudinal primary resonant case: $\mu_2 = \mu_3 = 0.165$, $\nu_1 = 0.1$, $r = 0.0245$, $\varepsilon = 0.2$, $\lambda_1 \cong \pi V$; (**a**) $\sigma_1 = 1$, $\sigma_2 = 0$, (**b**) $\sigma_1 = \sigma_2 = 0$

essentially the solution of the linear problem. Moreover, when a_1, b_2, and b_3 are all nonzero quantities by doing some mathematical simplifications the solution for a_1 amplitude becomes: $a_1 = \frac{2}{3\kappa}\{\mu_2\mu_3\omega_2\omega_3[1 + (\frac{\sigma_1+\sigma_2}{\mu_2+\mu_3})^2]\}^{1/2}$. It should be mentioned that similar relations exist for b_2 and b_3 and only for brevity we are not listing them. Nevertheless, the steady-state solutions for the b_2 and b_3 amplitudes are obtained implicitly using MATLAB solver package.

The variations of a_1, b_2, and b_3 amplitudes are plotted vs. parameter g, i.e., the amplitude of longitudinal excitation in Figs. 8 and 9. In Fig. 8, the so called saturation phenomenon for a_1 (a_{1s}) and jump phenomenon for a_1, b_2, and b_3 are shown. Moreover, the effect of nonlinearity for b_2 and b_3 curves is seen for g values around 0.21 (see Fig. 8a). In addition, variations for a_1, b_2, and b_3 represent multivaluedness in all g regions in this figure. In Fig. 8a, while the internal resonance is perfectly tuned, there is a small detuning of the external resonance, however, in Fig. 8b both of external resonance and internal resonance are perfectly tuned and that is why the unstable part (dashed regions) of b_2 and b_3 curves are converged to a single point around $g = 0.006$. The trend of a_1, b_2, and b_3 amplitudes changes vs. g can be pursued from two ways, i.e., from $g = 0$ to higher values and vise versa. These trends are chased in Figs. 8a and 8b by tracking red and blue arrows, respectively. As g increases from zero, so does a_1 until $g = 0.21$ where a_1 reaches to the value of a_{1s}, while b_2 and b_3 are still zero. This trend very well agrees with the results given by solution of the problem with the linear behavior. At this point, i.e., $g = 0.21$, any further increase in g will not produce further increase in a_1 because it makes (30) unstable.

To avoid instability condition beyond the $g = 0.21$, steady-state solutions should follow the nonzero solutions of (35) and (36). From this point onward, the

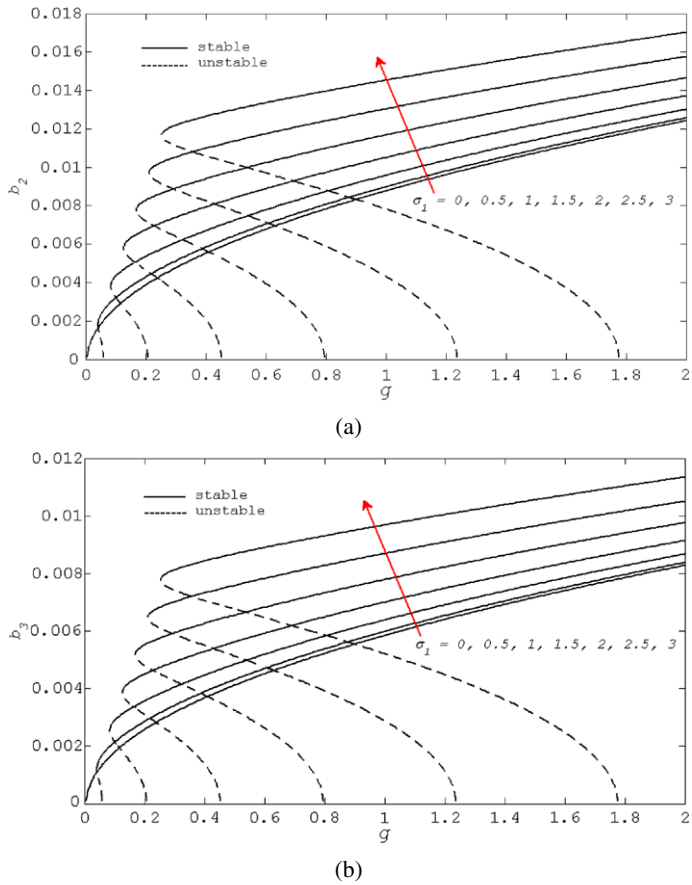

Fig. 9 Variation of nonzero b_2 and b_3 (amplitude response) vs. g for different σ_1 values $\mu_2 = \mu_3 = 0.165$, $\nu_1 = 0.1$, $r = 0.0245$, $\sigma_2 = 0$, $\varepsilon = 0.2$, $\lambda_1 \cong \pi V$; (**a**) b_2, (**b**) b_3

solution for a_1 yields to a flat line with the value of a_{1s} and for b_2 and b_3 it suddenly jumps from zero value to their upper corresponding curves, accordingly. Further increase in g causes a continuous increase in b_2 and b_3 as shown in Fig. 8a. When g decreases slowly from higher values to $g = 0$, primarily a_1 follows along a flat line which has a constant value of a_{1s} and the values of b_2 and b_3 decrease continually along their corresponding curves until $g = 0.08$. Further decrease in the value of g, causes the values of b_2 and b_3 to jump down from their corresponding bend points to a point on a flat line of $g = 0$ obtained by the linear solution given by (30). More reduction of g values will guide b_2 and b_3 to approach to the origin. At the same time, when a_1 by continuous decrease of g reaches to the point of $g = 0.08$, further reduction of g will cause the a_1 to jump down and then follow the appropriate ramp type variation. Upon further g reduction, a_1 moves toward the origin. These mechanisms of up and down variations of a_1, b_2, and b_3 are also depicted by directional arrows in Figs. 8a and 8b.

In the next step, we try to see the effect of σ_1 variation on the amplitude response of b_2 and b_3 curves. The results of this variation are illustrated in Fig. 9. It can be observed from this figure that any increase in the value of σ_1 will cause the significant displacement of the bent point to the higher value of g and corresponding amplitude.

There is still another parameter, σ_2, which its variation on the amplitude response should be considered. Figure 10 shows the effect of σ_2 variation on the amplitude response of b_2 and b_3 curves. It can be observed from this figure that a higher value of σ_2 has insignificant effect on the variation of b_2 and b_3.

In order to study the symmetric or unsymmetrical behavior frequency-response curve of nonlinear systems, one can analyze the variation of response curves vs. external resonance detuning parameter for a given g value. Figures 11a, 11b, and 11c represent these types of variations.

As it is seen from the Fig. 11a, when the internal resonance is perfectly detuning, i.e., $\sigma_2 = 0$, the sym-

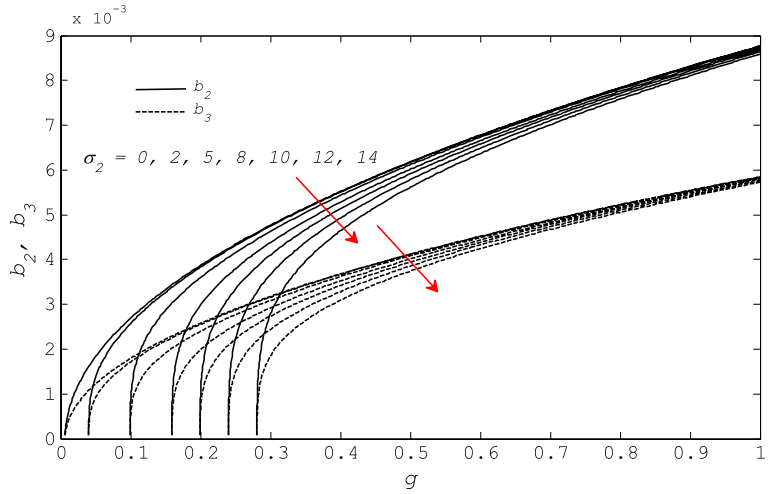

Fig. 10 Variation of nonzero b_2 and b_3 (amplitude response) vs. g for different σ_2 values $\mu_2 = \mu_3 = 0.165$, $\nu_1 = 0.1$, $r = 0.0245$, $\sigma_1 = 0$, $\varepsilon = 0.2$, $\lambda_1 \cong \pi V$

metric configuration is seen for the steady-state solutions with respect to the line $\sigma_1 = 0$. The nonzero value of σ_2 will cause the unsymmetrical conditions in frequency-response curves, more specifically in b_2 and b_3 curves as shown in Figs. 11b and 11c. Moreover, the jump phenomenon associated with the variation of the excitation frequency of the moving load is indicated by the directional arrows only in the Fig. 11a.

6 Conclusions

The nonlinear coupled longitudinal-transversal PDEs equations of motion of a pinned-pinned inclined Euler–Bernoulli beam subjected to a moving force are solved and the outcome results are as the following:

1. It can be seen that by increasing the beam's inclination angle the dynamic transverse displacement of the beam's mid-point decreases and, for example, at inclination angle of $\theta = 90°$, the dynamic lateral displacement becomes zero as expected.

2. It can be observed that at any velocity ratio, the dynamic displacement response of the linear and nonlinear solutions are almost the same for small values of the moving force and the maximum dynamic magnification factor (D_d) for linear and nonlinear solutions are the same, however, for larger values of the moving force the dynamic response of the beam using nonlinear theory has higher value than those given by linear theory, hence the difference between the dynamic displacement responses of the nonlinear and linear theories increase vividly.

3. By increasing the value of structural damping coefficient, the dynamic transverse displacement (w) decreases which is generally a natural phenomenon in any structural system.

4. It is concluded that the dynamic mid-point displacement of the beam using linear and nonlinear solutions are almost the same for the moving force values of $F \leq 10000$ N. However, for values of $F \geq 10000$ N, the magnitude of the transverse deflection (w) of the linear and nonlinear solutions differs and the difference becomes more as F increases. Also, it can be observed that the difference between the linear and the nonlinear solutions has an increasing trend up to the load velocity ratio of $\alpha = 1.2$ and a reverse trend for the load velocity ratio of $\alpha > 1.2$.

5. It has been noticed that by neglecting the nonlinear nature of the motion in an inclined beam and also the effect of the end slope one would get some error in the final target collision position.

6. Due to the existence of the quadratic nonlinearity nature of the coupled PDEs governing equations of motion, the system trend is like a soft spring. That is by increasing the magnitude of the moving load, the dynamic deflections become larger than those from solution of linear system.

7. Under steady-state condition and in the case of internal-external longitudinal primary resonance, out of amplitude-response curves there are two possible solutions: either longitudinal amplitude is nonzero and transversal amplitudes are zero, or both longitudinal and transversal amplitudes are all nonzero. That is, we have a jump phenomenon associated with this motion. In addition to the jump phenomenon, the saturation

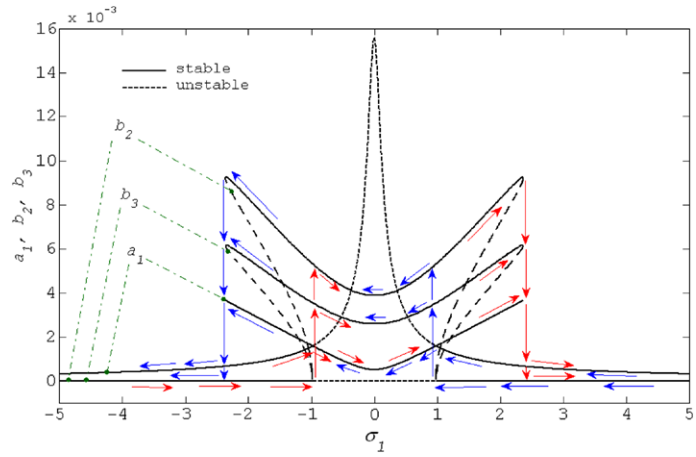

(a)

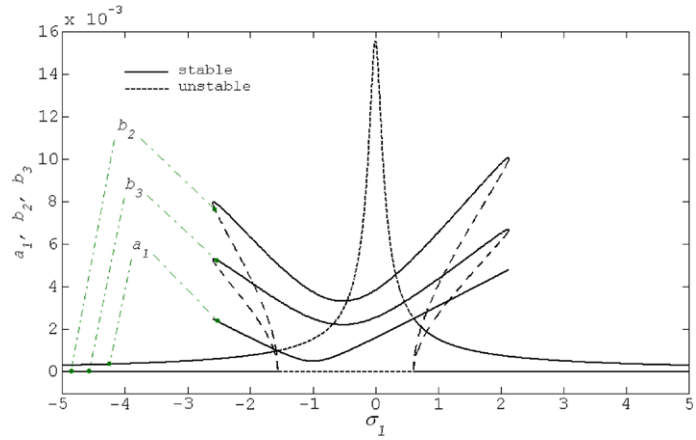

(b)

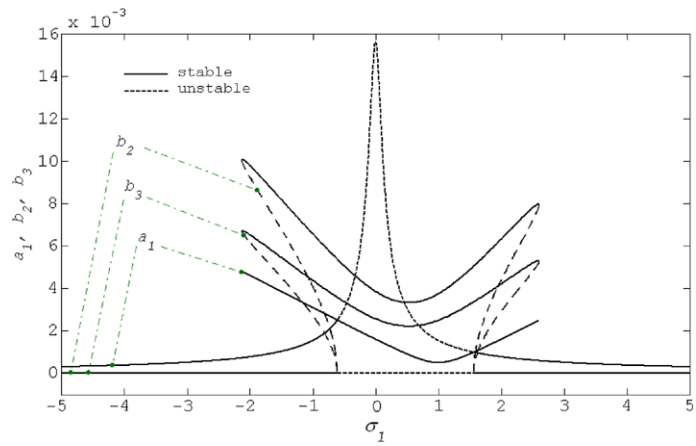

(c)

Fig. 11 Variation of a_1, b_2 and b_3 (frequency-response) vs. σ_1 for an inclined pinned-pinned beam under first longitudinal primary resonance case, $\mu_2 = \mu_3 = 0.165$, $\nu_1 = 0.1$, $r = 0.0245$, $\varepsilon = 0.2$, $\lambda_1 \cong \pi V$, $g = 0.2$; (**a**) $\sigma_2 = 0$, (**b**) $\sigma_2 = 1$, (**c**) $\sigma_2 = -1$

phenomenon is also associated with this motion. This means that by increasing either of external detuning or internal detuning parameters the stable region corresponded to the zero solutions for transverse amplitudes will be extended accordingly.

References

1. Abuhilal, M., Zibdeh, H.S.: Vibration analysis of beams with general boundary conditions traversed by a moving load. J. Sound Vib. **229**(2), 377–388 (2000)
2. Esmailzadeh, E., Ghorashi, M.: Vibration analysis of beams traversed by uniform partially distributed moving masses. J. Sound Vib. **184**(1), 9–17 (1995)
3. Esmailzadeh, E., Ghorashi, M.: Vibration analysis of a Timoshenko beam subjected to a traveling mass. J. Sound Vib. **199**(4), 615–628 (1997)
4. Foda, M.A., Abduljabbar, Z.: A dynamic green function formulation for the response of a beam structure to a moving mass. J. Sound Vib. **210**(3), 295–306 (1998)
5. Fryba, L.: Vibration of Solids and Structures Under Moving Loads. Thomas Telford, London (1999)
6. Ichikawa, M., Miyakawa, Y., Matsuda, A.: Vibration analysis of the continuous beam subjected to a moving mass. J. Sound Vib. **230**(3), 493–506 (2000)
7. Ju, S.H., Lin, H.T., Hsueh, H.H., Wang, S.H.: A simple finite element model for vibration analyses induced by moving vehicles. Int. J. Numer. Methods Eng. **68**, 1232–1256 (2006)
8. Kargarnovin, M.H., Younesian, D.: Dynamics of Timoshenko beams on Pasternak foundation under moving load. Mech. Res. Commun. **31**, 713–723 (2004)
9. Kargarnovin, M.H., Younesian, D., Thompson, D.J., Jones, C.J.C.: Response of beams on nonlinear viscoelastic foundations to harmonic moving loads. Comput. Struct. **83**, 1865–1877 (2005)
10. Kidarsa, A., Scott, M.H., Christopher, H.C.: Analysis of moving loads using force-based finite elements. Finite Elem. Anal. Des. **44**(4), 214–224 (2008)
11. Lee, H.P.: The dynamic response of a Timoshenko beam subjected to a moving mass. J. Sound Vib. **198**(2), 249–256 (1996)
12. Lin, Y.H., Trethewey, M.W.: Finite element analysis of elastic beams subjected to moving dynamic loads. J. Sound Vib. **136**(2), 323–342 (1990)
13. Lou, P., Dai, G.L., Zeng, Q.Y.: Finite-element analysis for a Timoshenko beam subjected to a moving mass. J. Mech. Eng. Sci., IMechE **220**(C), 669–678 (2006)
14. Michaltsos, G.T.: Dynamic behavior of a single-span beam subjected to loads moving with variable speeds. J. Sound Vib. **258**(2), 359–372 (2002)
15. Michaltsos, G., Sophianopoulos, D., Kounadis, A.N.: The effect of a moving mass and other parameters on the dynamic response of a simply supported beam. J. Sound Vib. **191**(3), 357–362 (1996)
16. Nayfeh, A.H., Mook, D.T.: Nonlinear Oscillations. Wiley-Interscience, New York (1979)
17. Olsson, M.: On the fundamental moving load problem. J. Sound Vib. **145**(2), 299–307 (1991)
18. Savin, E.: Dynamic amplification factor and response spectrum for the evaluation of vibrations of beams under successive moving loads. J. Sound Vib. **248**(2), 267–288 (2001)
19. Siddiqui, S.A.Q., Golnaraghi, M.F., Heppler, G.R.: Dynamics of a flexible beam carrying a moving mass using perturbation, numerical and time-frequency analysis techniques. J. Sound Vib. **229**(5), 1023–1055 (2000)
20. Simsek, M., Kocaturk, T.: Nonlinear dynamic analysis of an eccentrically prestressed damped beam under a concentrated moving harmonic load. J. Sound Vib. **320**, 235–253 (2009)
21. Thambiratnam, D., Zhuge, Y.: Dynamic analysis of beams on an elastic foundation subjected to moving loads. J. Sound Vib. **198**(2), 149–169 (1996)
22. Wang, R.T.: Vibration of multi-span Timoshenko beams to a moving force. J. Sound Vib. **207**(5), 731–742 (1997)
23. Wang, R.T., Chou, T.H.: Non-linear vibration of Timoshenko beam due to moving force and the weight of beam. J. Sound Vib. **218**(1), 117–131 (1998)
24. Wang, R.T., Lin, J.S.: Vibration of multi-span Timoshenko frames due to moving loads. J. Sound Vib. **212**(5), 417–434 (1998)
25. Wu, J.J.: Dynamic analysis of an inclined beam due to moving loads. J. Sound Vib. **288**, 107–133 (2005)
26. Xu, X., Xu, W., Genin, J.: A non-linear moving mass problem. J. Sound Vib. **204**(3), 495–504 (1997)
27. Yanmeni Wayou, A.N., Tchoukuegno, R., Woafo, P.: Nonlinear dynamics of an elastic beam under moving loads. J. Sound Vib. **273**, 1101–1108 (2004)
28. Younesian, D., Kargarnovin, M.H., Thompson, D.J., Jones, C.J.C.: Parametrically excited vibration of a Timoshenko beam on random viscoelastic foundation subjected to a harmonic moving load. Nonlinear Dyn. **45**, 75–93 (2006)